

A STUDY OF TEMPERATURE FLUCTUATIONS  
AND THEIR STATISTICS IN TURBULENT  
CONVECTION

By

GEORGE KAMBOUROGLOU

Bachelor of Arts

Illinois Wesleyan University

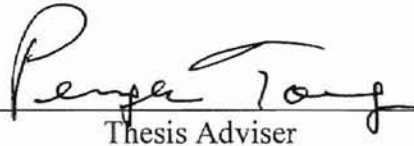
Bloomington, Illinois

1993

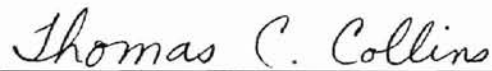
Submitted to the Faculty of the  
Graduate College of the  
Oklahoma State University  
in partial fulfillment of  
the requirements for  
the Degree of  
MASTER OF SCIENCE  
August, 1997

A STUDY OF TEMPERATURE FLUCTUATIONS  
AND THEIR STATISTICS IN TURBULENT  
CONVECTION

Thesis Approved:

  
Thesis Adviser

  
B

  
Dean of the Graduate College

## ACKNOWLEDGEMENTS

I wish to express my sincere thanks to all the people who have contributed in many ways in making this thesis possible.

First, my most sincere thanks must go to my adviser, Dr. Penger Tong, for his help, encouragement, guidance, and most of all the patience he has shown with me, during the past three years. I have been most fortunate to have worked in his excellent laboratory, and have learnt a great deal in instrumentation and data acquisition. I feel a lot more confident about my abilities after these last few years. I am also most grateful to my committee members, Dr. Bruce J. Ackerson and Dr. Joel Martin, for their careful review of my thesis and the time they have devoted to my thesis defense.

I would also like to express my gratitude to all members of our group, past and present. Dr. Yi Shen, Dr. Theyencheri Narayanan, Mr. Xe Yi, and Ms. Yibing Du have all helped immensely, and have been great friends to me. Mr. Ulf Nobbmann is another person who has stood by me, when at times things looked bleak, and provided me with the strength and courage that made this thesis possible. I would be amiss not to thank a few other good friends and classmates who have also helped at one time or another, throughout my stay here at Oklahoma State University. A big thank you goes to Mike and Linda Clark, Brian Little, Dan Bloom, Anne Georgalas, Sheng Xu, Mike Furlough, John

Snodgrass, Chip Holden, Sheena Jacob, Steve Willoughby, Von Whitley, Mike Humphrey, Art Fischer, and Mark O'Steen.

Special thanks go to my parents Jordan and Lina, and my brother Gabriel, whose love and support have been unbelievable at times! My mother has stood by me through these tough years, even though she is thousands of miles away.

I dedicate this thesis to her.

## TABLE OF CONTENTS

Chapter	Page
1. INTRODUCTION .....	1
1.1 Background.....	1
1.2 Rayleigh-Bénard Convection.....	2
2. EXPERIMENTAL PROCEDURES AND APPARATUS.....	9
2.1 Rayleigh-Bénard Cell.....	9
2.2 Data Acquisition.....	12
3. EXPERIMENTAL RESULTS .....	22
4. CONCLUSIONS.....	36
BIBLIOGRAPHY.....	38

## LIST OF FIGURES

Figure	Page
1. Flow states of thermal convection.....	5
2. Bénard convection cell.....	9
3. Schematic diagram of experimental setup.....	11
4. Front Panel of Keithley 2001 VI.....	18
5. Block Diagram of Keithley 2001 VI.....	19
6. Front Panel of Keithley 199 VI.....	20
7. Block Diagram of Keithley 199 VI.....	21
8. Nusselt number as a function of Rayleigh number.....	23
9. Resistance variations $R_t$ with time $t$ at the center of the cell.....	24
10. Measured temperature PDF at $Ra = 1.09 \times 10^{10}$ .....	26
11. Measured temperature PDF for different $Ra$ .....	28
12. Measured power spectrum $S(\omega)$ at $Ra = 1.09 \times 10^{10}$ .....	29
13. Measured power spectra $S(\omega)$ in two different cells at approximately equal Rayleigh numbers.....	30
14. Measured temperature PDF's in two different cells at approximately equal Rayleigh numbers.....	31
15. Measured temperature rms as a function of $Ra$ .....	35

## LIST OF TABLES

Table	Page
I. Results of the heat transport measurements carried out in the 20 cm "smooth" cell.....	22

# CHAPTER 1

## INTRODUCTION

### 1.1 Background

In the field of fluid dynamics, turbulence presents one of the most challenging problems to understand. Turbulence, a common natural phenomenon, is associated with both spatial and temporal random fluid motions. Because of this random nature, and the non-linearity of the Navier-Stokes equation which describes the fluid motion, turbulence remains as an essentially unsolved problem in classical physics.

There have been many theories and statistical methods employed to describe turbulence. Among them, the most far-reaching theory of turbulence was proposed by Kolmogorov, in 1941 [9]. In his theory, boundaries are assumed to be at infinity and the flow is isotropic and homogenous. This model is regarded as a good description of fully developed turbulence. However, in many flow systems, boundaries are always part of the whole turbulence problem, and they cannot be simply ignored. Also, in many experiments, coherent structures are observed which have characteristic length scales comparable with the size of the system.

Our aim, in this thesis, is to study turbulence in a flow system with well defined boundary conditions, and the flow can be changed to a turbulent state in a controlled manner.



Thermal convection meets our demands and goals. In experimental terms, it is simply a horizontal fluid layer, heated from below. The boundary conditions are rather simple and experimentally easy to impose: fix the top of the fluid layer at one temperature and the bottom at a higher one. By varying the size of the cell or the temperature drop across the cell, or even the fluid properties, one is able to study, in such a closed box, how a flow evolves from laminar to turbulent.

## 1.2 Rayleigh-Bénard Convection

An example of thermal convection is Rayleigh-Bénard convection, named after Bénard [1], who first performed experimental studies in 1901, and Rayleigh [15] who performed theoretical calculations in 1916. In a thermal convection, the flow state is characterized by the dimensionless Rayleigh number ( $Ra$ ) as follows:

$$Ra = \frac{\alpha g h^3 \Delta T}{\nu \kappa_d}, \quad (1)$$

where:  $\alpha$  is the thermal expansion coefficient,  
 $g$  is the gravitational acceleration,  
 $h$  is the height of the convection cell,  
 $\Delta T$  is the temperature difference between the upper and lower plates,  
 $\nu$  and  $\kappa_d$  are the kinematic viscosity and thermal diffusivity of the convecting fluid (in our case water), respectively.

The Rayleigh number can also be expressed as the ratio of the buoyancy contribution to the diffusion contributions [17],

$$Ra = \frac{\tau_v \tau_t}{\tau_b^2}, \quad (2)$$

where:  $\tau_t \sim h^2/\kappa_d$  is the thermal diffusivity time;

$\tau_v \sim h^2/\nu$  is the viscous diffusion time;

and  $\tau_b \sim (h/a)^{\frac{1}{2}} \sim \left(\frac{h}{g\alpha\Delta T}\right)^{\frac{1}{2}}$  is the time for the buoyant force to move

the fluid from the lower plate to the upper plate.

The Rayleigh number is one of the control parameters in thermal convection. Another quantity of interest is the Nusselt number ( $Nu$ ). It is a measure of the heat transport efficiency, and thus reflects the changes of turbulent states as well.  $Nu$  is defined as the total heat flux,  $q_{total}$ , transferred vertically through the cell, normalized by the pure conductive heat flux,  $q_c = k_w\Delta T/h$ , where  $k_w$  is the thermal conductivity of the fluid [17]. Hence, the Nusselt number is given by the following equation:

$$Nu = \frac{q_{total}}{\Delta T k_w / h}. \quad (3)$$

In the same fashion, the third control parameter for a thermal convection experiment is the Prandtl number  $Pr$ , defined as

$$Pr = \frac{\nu}{\kappa_d}. \quad (4)$$

The Prandtl number can also be expressed in terms of the ratio of the thermal diffusion time to the viscous diffusion time [17],

$$Pr = \frac{\tau_t}{\tau_v}. \quad (5)$$

It is important to note that different fluids with the same values of  $Ra$  and  $Pr$  will have a similar flow behavior, because the fluid parameters enter the equation of motion only through these two dimensionless numbers. In a thermal convection experiment, both the Rayleigh number  $Ra$  and the Prandtl number  $Pr$  are well controlled, as well as the aspect ratio  $A=D/L$ , where  $D$  and  $L$  are the cell diameter and height, respectively. In the experiment to be described below we vary  $Ra$  while keeping  $Pr$  and  $A$  unchanged, a method which has been used by many recent experimental studies [10] [19] [22] [23] [24]. In these experiments, attention has been focused on characterizing the flow states of the convection over varying  $Ra$  [10]. As  $Ra$  is increased from  $10^3$  to  $10^{13}$ , the fluid motion undergoes transition to different states, from pure convection to turbulence (see Figure 1) [10] [17]. Libchaber et al. have characterized the flow states by measuring the Nusselt number,  $Nu$ , as a function of the Rayleigh number  $Ra$  at a constant  $Pr$  [23].

In order to distinguish the behavior between relatively low Rayleigh numbers from that for higher Rayleigh numbers (up to the values studied), Libchaber et al. have called the former soft turbulence and the latter hard turbulence. Temperature fluctuations and their statistics are very different in the two turbulent states. In the soft turbulence regime, the temperature probability density function (PDF) in the middle of the cell is of Gaussian form; whereas in the hard turbulence regime, the temperature PDF decreases exponentially on either side of the mean value. This statistical behavior of temperature fluctuations is found everywhere in the central region of the convection cell [10].

In our experiment the Rayleigh number,  $Ra$ , was varied between  $10^8$  and  $10^{10}$ . In this  $Ra$  range, the fluid motion starts at the upper end of the “soft” turbulence regime and extends well into the “hard” turbulence regime.

Getting back to the fundamental underlying principles behind Rayleigh-Bénard convection, one can easily see the process that takes place in thermal convection. When a horizontal layer of fluid is heated from below, Rayleigh-Bénard convection occurs if the

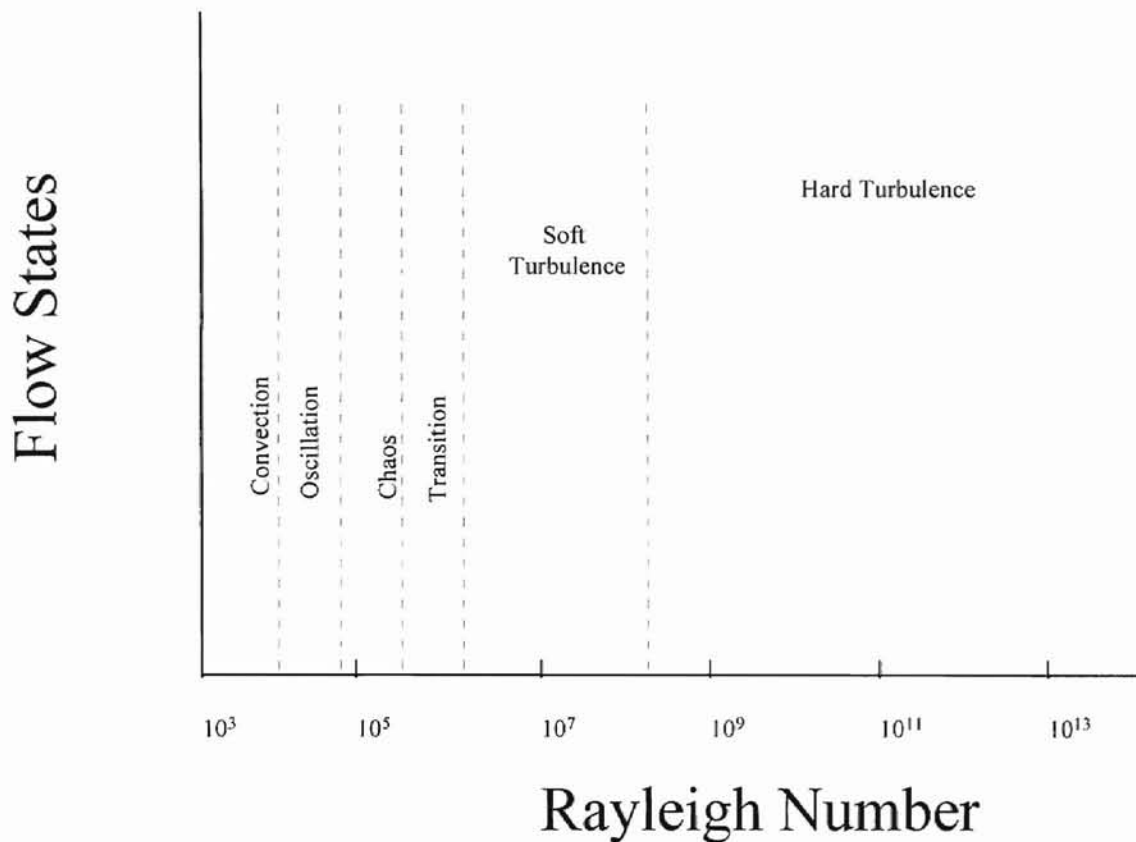


Figure 1. Flow states of thermal convection at a different Rayleigh number, ranging from  $Ra = 10^3$  to  $10^{13}$  (adapted from [10]).

temperature difference  $\Delta T$  across the layer exceeds a critical value  $\Delta T_c$ . Because of the buoyancy effect due to gravity, the cooler fluid on the top of the fluid layer will begin moving downward, and the warmer fluid on the bottom of the fluid layer will begin moving upward. In this manner a convection flow is established in the cell. As an incompressible fluid in closed surroundings, the equations of motion that govern Rayleigh-Bénard convection are as follows:

Incompressibility equation:

$$\nabla \cdot \mathbf{v} = 0. \quad (6)$$

Momentum equation:

$$\left( \frac{\partial \mathbf{v}}{\partial t} + \mathbf{v} \cdot \nabla \mathbf{v} \right) = \nu \nabla^2 \mathbf{v} - \nabla p / \rho_0 - \alpha \Delta T g \hat{z}. \quad (7)$$

Heat equation:

$$\left( \frac{\partial T}{\partial t} + \mathbf{v} \cdot \nabla T \right) = \kappa_d \nabla^2 T. \quad (8)$$

where:

- $\mathbf{v}$  is the unknown velocity field;
- $p$  is the unknown pressure field;
- $T$  is the unknown temperature field;
- $\rho_0$  is the density of the fluid;
- $g$  is the gravitational acceleration;
- $\nu$  is the kinematic viscosity;
- $\kappa_d$  is the thermal diffusivity;

$\alpha = \frac{1}{\rho} \frac{\partial \rho}{\partial T}$  is the thermal expansion coefficient; and

$\Delta T = T_{bottom} - T_{top}$  is the temperature difference between the upper and lower plates.

The vertical coordinate is denoted as  $\hat{z}$  with the positive direction pointing upwards.

We have used the Boussinesq approximation in obtaining the above equations [21]. Under the Boussinesq approximation, variations of all fluid properties versus temperature, other than the density, are ignored completely [5]. The time averaged density variation is so small compared to the density itself that one may neglect its effect in all terms of the equations except for the buoyancy term. Eq. (6) is obtained from the mass conservation equation,  $\frac{\partial \rho}{\partial t} + \nabla \cdot (\rho \mathbf{v}) = 0$ , simplified under the Boussinesq approximation. Eq. (7) is the Navier-Stokes equation with the external force being the net buoyancy force  $\alpha \Delta T g \hat{z}$ . Finally, Eq. (8) is the heat equation for thermal convection.

For turbulent convection, the unknown fields  $\mathbf{v}$ ,  $p$ , and  $T$  are coupled together. Furthermore, the nonlinear operator,  $(\mathbf{v} \cdot \nabla) \mathbf{v}$  makes it quite difficult to find exact solutions for the equations. However, one can use scaling arguments to analyze the convection problem. Using the temperature difference,  $\Delta T$ , the cell height  $h$ , and the typical diffusion time  $h^2/\kappa_d$ , as the scaling variables for the temperature  $T$ , the length  $L$ , and the time  $t$ , one may rewrite Eqs. (6), (7), and (8) in dimensionless forms:

$$\nabla \cdot \mathbf{v} = 0. \quad (9)$$

$$\frac{\partial T}{\partial t} + \mathbf{v} \cdot \nabla T = \nabla^2 T. \quad (10)$$

$$\frac{1}{Pr} \left( \frac{\partial \mathbf{v}}{\partial t} + \mathbf{v} \cdot \nabla \mathbf{v} + \nabla p \right) = \nabla^2 \mathbf{v} + Ra T \hat{z}. \quad (11)$$

The above equations require boundary conditions for the temperature and the velocity fields. The most common type specifies the temperature at the surrounding walls [6]. There are, however, other types. As an example we may mention the case in which the heat transfer through a wall is specified. In our case, the boundary conditions are:

- (1)  $\mathbf{v}_{sidewalls} = \mathbf{v}_{plates} = 0$ , (nonslip boundary condition);
- (2)  $T_{top} = 1/2$ ,  $T_{bottom} = -1/2$ , (regulated temperature at the upper and lower plates); and
- (3)  $(\nabla T \cdot \hat{n})_{sidewalls} = 0$  (no heat flux leakage at the sidewalls).

Eq. (11) illustrates that solutions for the velocity  $\mathbf{v}(\mathbf{x}, t)$ , temperature  $T(\mathbf{x}, t)$ , and pressure  $P(\mathbf{x}, t)$ , only depend on the dimensionless Rayleigh number and the Prandtl number. The aspect ratio  $A$  enters the problem through the boundary conditions.

It should be emphasized that thermal conduction plays an integral role in convection. For example, when heat is introduced into a fluid by heating a boundary wall, there is no advection of heat near the boundary; the fluid first gains heat entirely by conduction, although further away from the wall, advection may be the principal process. The traditional division of heat transfer processes into radiation, conduction, and convection is not completely sharp. Whenever convection occurs, conduction and convection become parts of a single process [4].

# CHAPTER 2

## EXPERIMENTAL PROCEDURES AND APPARATUS

### 2.1 Bénard Cell

In this chapter we discuss the experimental setup, the equipment used and the data acquisition techniques which played a *pivotal* role in the completion of this project.

Fig. 2 shows the typical convection cell used in the experiment, which consisted of two brass plates (top and bottom), electroplated with a thin layer of gold to prevent rust.

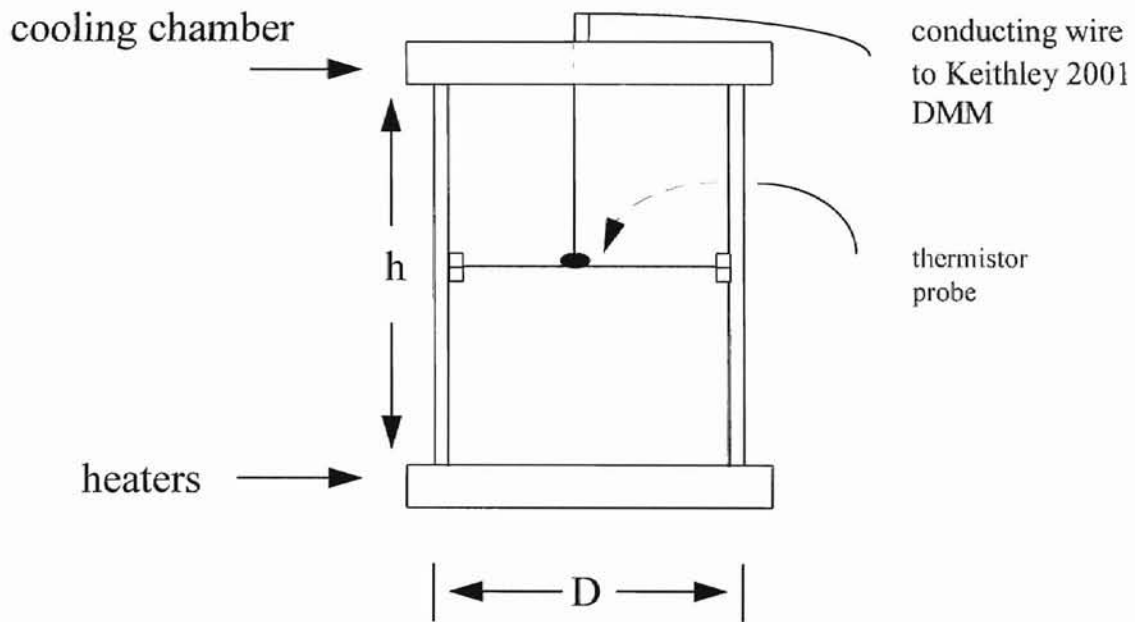


Figure 2. Bénard convection cell.



The main "body" of the cell was a cylindrical ring made of transparent Plexiglas. A Thermometrics 103L thermistor was mounted on a supporting wire at the center of the ring, in order to measure the temperature at that particular point. Two cylindrical cells with the same inner diameter of 20 cm, but different heights of 20 and 40 cm were used, respectively, in order to obtain a wider range of the Rayleigh number ( $Ra$ ). The aspect ratios, defined in the previous chapter, for the aforementioned cells were 1.0 and 0.5, respectively.

The top plate was kept at a constant temperature, controlled by a flow-through cooler and a circulator (both manufactured by NESLAB) which pumped a 2°C mixture of water and ethylene glycol through the cooling chamber, mounted on the upper part of the top plate. The bottom plate of the cell was uniformly heated at a constant rate by two circular silicone rubber electric heating films (Model SRFR 7/10 manufactured by OMEGA). These two heaters were sealed with conducting paste to ensure the best possible uniformity in heating, and "sandwiched" between two copper plates on the back side of the bottom plate. The electric resistance of each heater was 33.4Ω and the total resistance of the two heaters connected in parallel was 16.7Ω. A DC power supply (manufactured by SORENSEN) with a long-term stability of 0.1% provided the electric current. Two OMEGA 44031 thermistors were embedded in the top and bottom plates to monitor their temperatures. The temperature of the top plate was stable to within 0.15 °C and that of the bottom plate was stable to within 0.1 °C.

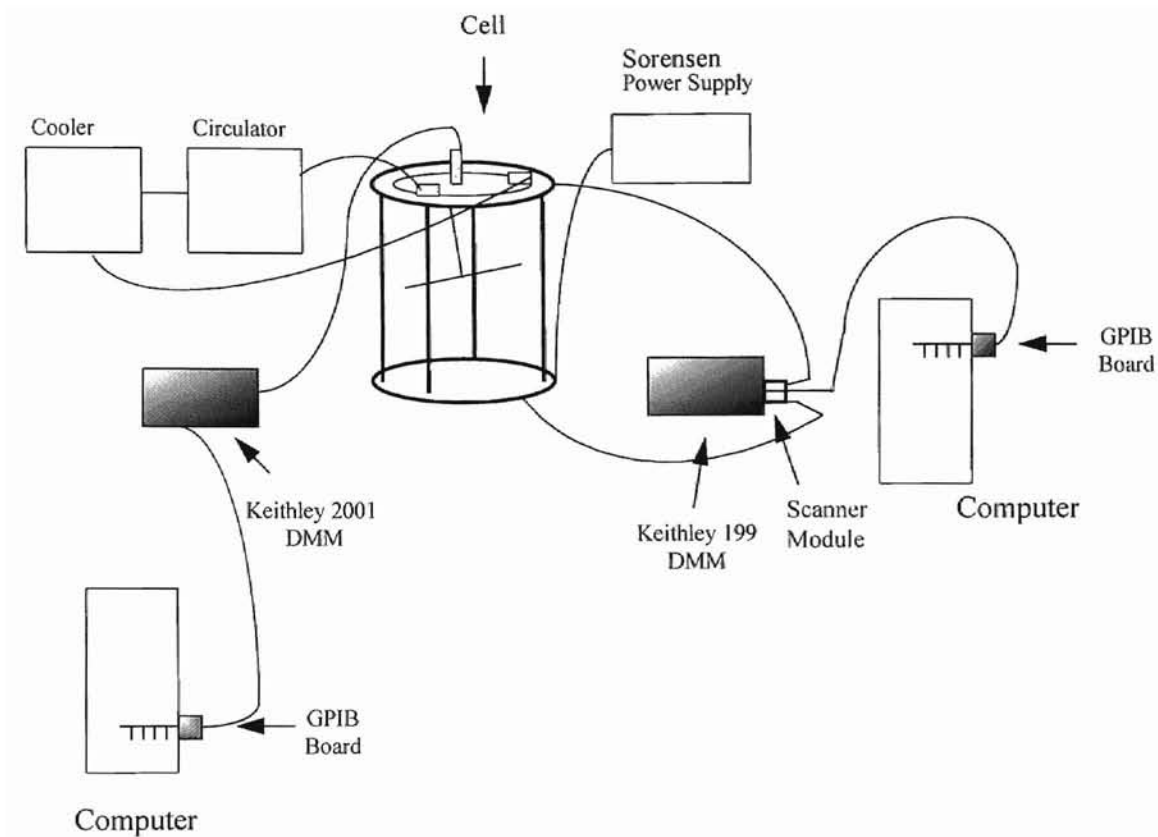


Figure 3. Schematic diagram of experimental setup.

Fig. 3 illustrates the experimental setup. The different wire connections are indicated as well as their locations on the main convection cell. Note that there are two wires from Keithley 199 DMM attached to the cell, aided by the multi-channel scanner module.

The heat transport across the convection cell is characterized by the Nusselt number  $Nu$ , which is defined as the ratio of the total vertical heat flux across the cell to the heat flux carried by pure conduction. The total heat flux was determined by the input electric power,  $V^2/R$ , that was required to maintain the lower plate at a constant temperature. Here,  $V$  is the dc voltage applied to the heater embedded in the bottom plate

and  $R = 16.7\Omega$  is the total resistance of the heating films as mentioned before. In our thermal measurements, great care was taken to ensure that the convection cell is well insulated. A square box made of polystyrene Styrofoam was used to surround the cell and the empty space in-between was filled with gold fiber glass to avoid heat leakage to the surroundings. We used two kinds of convection cells in the experiment; one kind is the "smooth" cell and the other kind is the "rough" cell. The top and bottom plates of the rough cells were made of the same brass plates as those used in the smooth cells, but had woven V-shaped grooves on them. The grooves had a vertex angle of  $90^\circ$  and their spacing was such that a square lattice of pyramids was formed on the surface. The height of the pyramids (the roughness height  $h_0$ ) was 9.0 mm and their spacing  $s = 18.0$  mm. For the entire  $Ra$  region in our experiment, the roughness height  $h_0$  remains larger than the thermal boundary layer thickness,  $h > \delta_{th}$ . In this case, the surface roughness is expected to strongly affect temperature fluctuations near the surface and thereby alter the heat transport across the cell. In theories of the heat transport in turbulent convection, one often assumes that the thermal boundary layer is marginally stable, i.e., its thickness grows to an average value of  $\delta_{th}$ , then it becomes unstable to thermal eruptions [18].

## 2.2 Data Acquisition

As was mentioned before, data acquisition is essential to the success of the project. Because a large number of data sets is needed to ensure the best possible statistics, automatic data acquisition using a computer is employed in this experiment.

Two National Instruments AT-GPIB/TNT™ Interface Boards (heretofore referred to as GPIB boards) along with the NI-488.2™ and LabVIEW® software packages were used, in connection with a KEITHLEY Model 2001 and a KEITHLEY Model 199 digital multimeters. The software packages and the GPIB boards were installed in two GATEWAY 2000 Pentium personal computers, which have a clock speed of 90 MHz. The actual preparation of the data acquisition system was rather complex and involved a number of steps. More specifically, the configuration of the GPIB boards involved the matching of the factory-default settings of the two digital multimeters and their specifications regarding the speed (or rate) of data transfer, the format of data (binary or ASCII) and its size. An item of concern at the initial stage of the board configuration was that the hardware interrupt request lines and the input/output addresses (in hexadecimal) of both GPIB boards had to be modified in order to successfully communicate with the multimeters. This was done in two steps. The first step involved the manual alteration of configuration jumpers and switches on the boards, while the second one involved the use of the accompanying software package NI-488.2 with the diagnostics tool, *ibdiag*, and the configuration tool, *ibconf*. Another problem we encountered was related to the enabling of the direct memory access (DMA), with which one can directly transfer the data from devices, such as the GPIB board, to the computer memory. In most cases, DMA transfers the data much faster than the programmed I/O does [14]. Again, we had to alter the default factory settings of the boards due to conflicts with other devices present in both computers. With the direct memory access, we were able to achieve a maximum GPIB

transfer rate up to 1.5 Mbytes/s, although the actual speed varied considerably due to the system and instrumentation capabilities.

Once the hardware connections were accomplished, the interfacing software LabVIEW was used to control the instruments and to store the data in the computer. Before we proceed, it would be useful to briefly describe the inner-workings of LabVIEW in order to appreciate its capabilities.

LabVIEW in essence is a program development application, very much like C or BASIC [12]. However, LabVIEW is different from those applications in that it uses a *graphical* programming language, *G*, to create programs in block diagram form whereas the other programming systems use *text-based* languages to create lines of code. Like C or BASIC, LabVIEW is a general-purpose programming system with extensive libraries of functions and subroutines for many programming tasks. In particular, LabVIEW contains application-specific libraries for data acquisition, GPIB and serial instrument control, and extensive statistical package and data storage routines. Its programs are called *virtual instruments (VI's)*, because their appearance and operation mimic actual instruments used in the laboratory environment, such as digital multimeters.

The user interface of a VI is called the *front panel*, and can be made to resemble the user interface of a physical instrument. This feature is mainly a combination of controls and indicators, knobs, push buttons, graphs, etc. A user inputs control commands and data using a mouse or a keyboard and then views the results on the computer screen. Controls simulate instrument input devices and supply data to the block diagram, which is a pictorial solution to a particular programming problem, as well as being the source

code for the VI. Indicators simulate instrument output devices that display data acquired or generated by the block diagram of the VI.

The Diagram window holds the block diagram of a VI, which is the *backbone* of a the LabVIEW VI. It can be constructed by *wiring* together objects that send or receive data, perform specific functions, and control the flow of execution. One of the great advantages for LabVIEW is that debugging source code is greatly simplified by visual tools that locate problematic segments of the program, in addition to offering user-friendly suggestions for alternative commands [13].

Several VI's have been constructed to match the needs and goals of this experiment. Some of the VI's were originally programmed by KEITHLEY but were greatly modified, in order to achieve our specific demands. In particular, we have decided that the data will be stored initially in the buffer of the instrument and then transferred via GPIB to the computer. ASCII format was used for the storage of the actual resistance values of the thermistor, and these resistance values were recorded without their respective time-stamps. Although a binary format is more suitable for fast data transfers, its inherent difficulties with spreadsheet programs prohibit us from using it. The KEITHLEY 2001 digital multimeter was used to measure the resistance changes of the thermistor due to the temperature fluctuations at the center of the convection cell. The temperature (resistance) data were broken into files and each one of them contained 29899 data points (the maximum number allowed by the multimeter). For a given  $Ra$ , we typically collected 15 data files (3-4 hours of data taking in real time) with two different sampling rates, 20 Hz and 35 Hz. The sampling rates were chosen to pick up temperature

fluctuations with the highest frequency present in the signal [7]. Another concern was that the 2001 model has an automatic *zero* function with which one controls the frequency of automatic zero readings taken. When the automatic *zero* setting is disabled (to increase the sampling rate), internal calibration and zeroing will be affected by changes in the input signal. To reduce measurement errors, we decided to use the so-called "normal" auto zero setting which was automatically performed whenever necessary to achieve the specified accuracy. This accuracy is also related to the integration time of the A/D converter used in the instrument. The integration time is the period of time during which the input signal is measured, and is also known as the aperture [7]. Since the integration time affects the resolution of the measurement and the ultimate sampling rate, it was optimized to 16.67 msec, which is 1.0 power line cycles (1.0 PLC).

In order to obtain a high statistical accuracy the virtual instrument (VI) controlling the KEITHLEY 2001 Model was further modified, such that one could obtain a large number of data files by simply entering the "path location" (referring to the appropriate sub-directory in the hard drive), the number of files (in our case 15) and the file extension (e.g. ".dat") on the appropriate control in the front panel. A graph of the measured resistance (temperature) vs. time is also added such that one can directly see the measured temperature fluctuations for a given sequence of files. We use the "Write To Spreadsheet File" VI provided by the LabVIEW analysis package, to convert the measured 1-D array of single precision resistance values to a text string and then write the string to a new ASCII file or to an existing file [13]. This VI is very useful since it creates a text file

readable by most spreadsheet applications. Figures 4 and 5 show the final front panel and block diagram of the Keithley 2001 VI.

A similar VI was constructed for the KEITHLEY 199 Model (Figures 6 and 7). Once again, one can specify the number of files to be sampled, the sampling rate, and the path location in which the data files are stored. In addition, we took full advantage of the scanning capability of the multimeter. With the multiple (2) input channels on the back panel of the multimeter, we can simultaneously measure the temperatures of both the top and bottom plates of the convection cell [8]. The measurements were carried out, over a long period of time (in excess of three hours), to monitor the temperature stability of the system. Two chart graphs were added to the VI to provide visual records of the temperature fluctuations of the top and bottom plates.



Front Panel

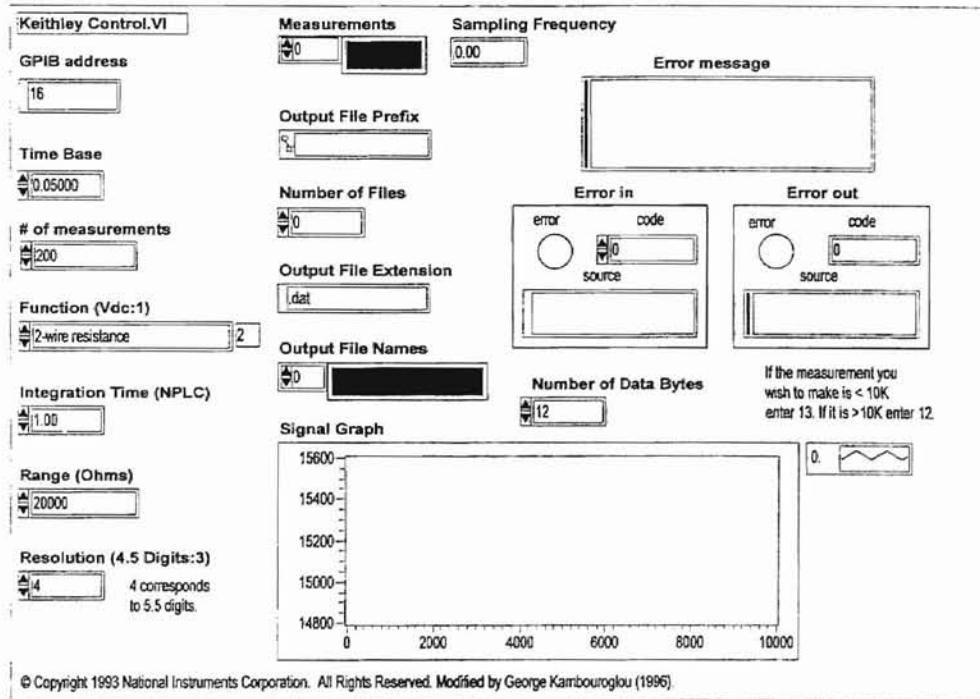


Figure 4. Front Panel of Keithley 2001 VI

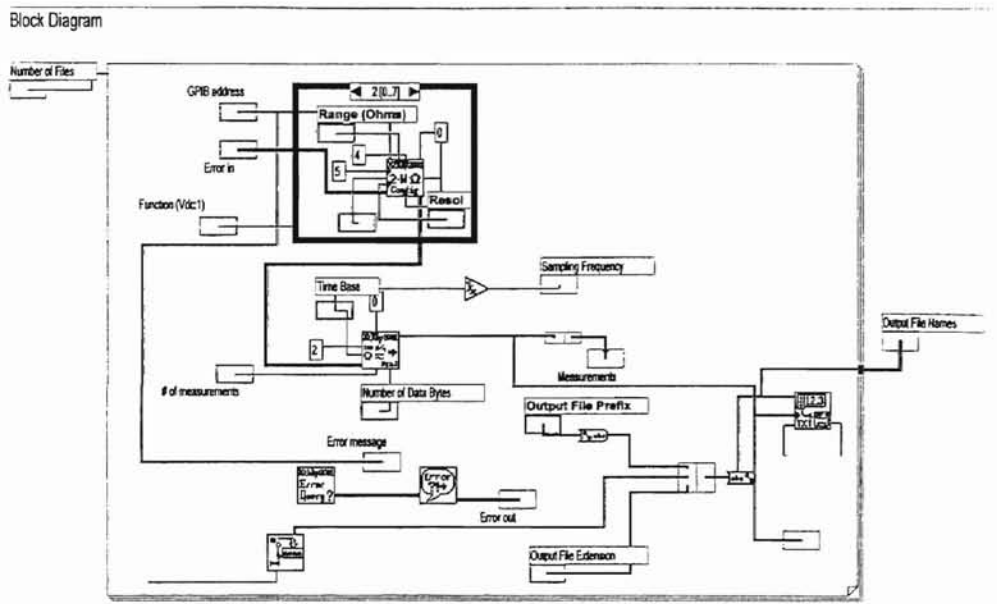


Figure 5. Block diagram of Keithley 2001 VI

Front Panel

### KEITHLEY 199 SYSTEM DMM / SCANNER

**GPIB address**   
26

**Channels**   
2 Channels

**Function (DCV:0)**   
resistance

**Pole/ratio**   
2-pole

**Range (auto:0)**   
Autorange

**Scan Interval (msec)**   
6000

**Delay value msec**   
10

**Number of points**   
5000

**File Path**   
%s

**Readings from Ch. 1**   
0

**Readings from Ch. 2**   
0

**Channel 1 Average**  Ch. 1  $\sigma$   
0.00 0.00

**Channel 2 Average**  Ch. 2  $\sigma$   
0.00 0.00

**error out**   
error code  
source

**error in**   
error code  
source

**Graph 1**   
4090  
4085  
4080  
4075  
4070  
4065  
0 10 20 30 40 50 60 70 80 90 99

**Graph 2**   
17350  
17325  
17300  
17275  
17250  
17225  
17200  
17175  
0 10 20 30 40 50 60 70 80 90 99

© Copyright 1993 National Instruments Corporation. All Rights Reserved.  
Modified by George Kambourgou, 3/1996.

Figure 6. Front Panel of Keithley 199 VI

Block Diagram

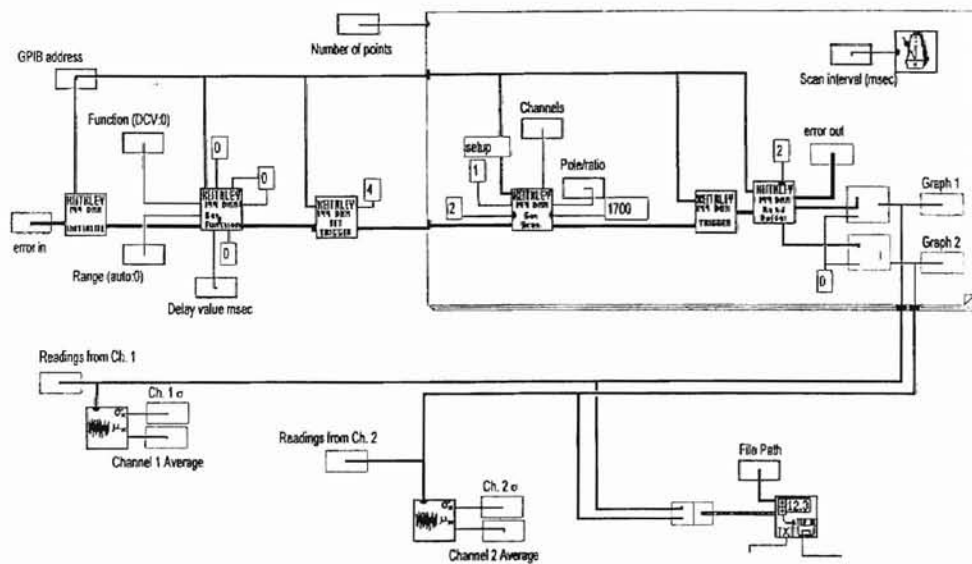


Figure 7. Block diagram of Keithley 199 VI

# CHAPTER 3

## EXPERIMENTAL RESULTS

We now present our temperature measurements at the center of the convection cell. We first discuss the measurements carried out in the 20 cm and 40 cm “smooth” cells. We then compare the results obtained from the “smooth” cells with those from the “rough” cells at different Rayleigh numbers.

We focus our attention at the center of the cell, where the flow is believed to be characteristic of free convection. Results of the heat transport measurements are summarized in Table I.

TABLE I  
Results of the heat transport measurements carried out  
in the 20 cm “smooth” cell.

Heating Voltage (V)	$\Delta T$ (°C)	$Ra$	$Nu$
20	8.751	$2.16 \times 10^8$	30.0295
30	13.454	$6.23 \times 10^8$	43.6166
40	18.741	$1.39 \times 10^9$	54.8781
50	24.452	$2.65 \times 10^9$	64.9677
60	30.189	$4.58 \times 10^9$	74.8593
70	36.483	$7.37 \times 10^9$	83.1293
80	42.537	$1.09 \times 10^{10}$	91.7877
90	48.844	$1.56 \times 10^{10}$	100.626

Figure 8 shows the measured  $Nu$  as a function of  $Ra$  in the smooth cells with  $A = 0.5$  and  $A = 1.0$ . It is seen that the data can be well described by the power law (solid line)  $Nu = 0.132 \times Ra^\epsilon$ . The measured exponent is  $\epsilon = 0.286$  which agrees well with

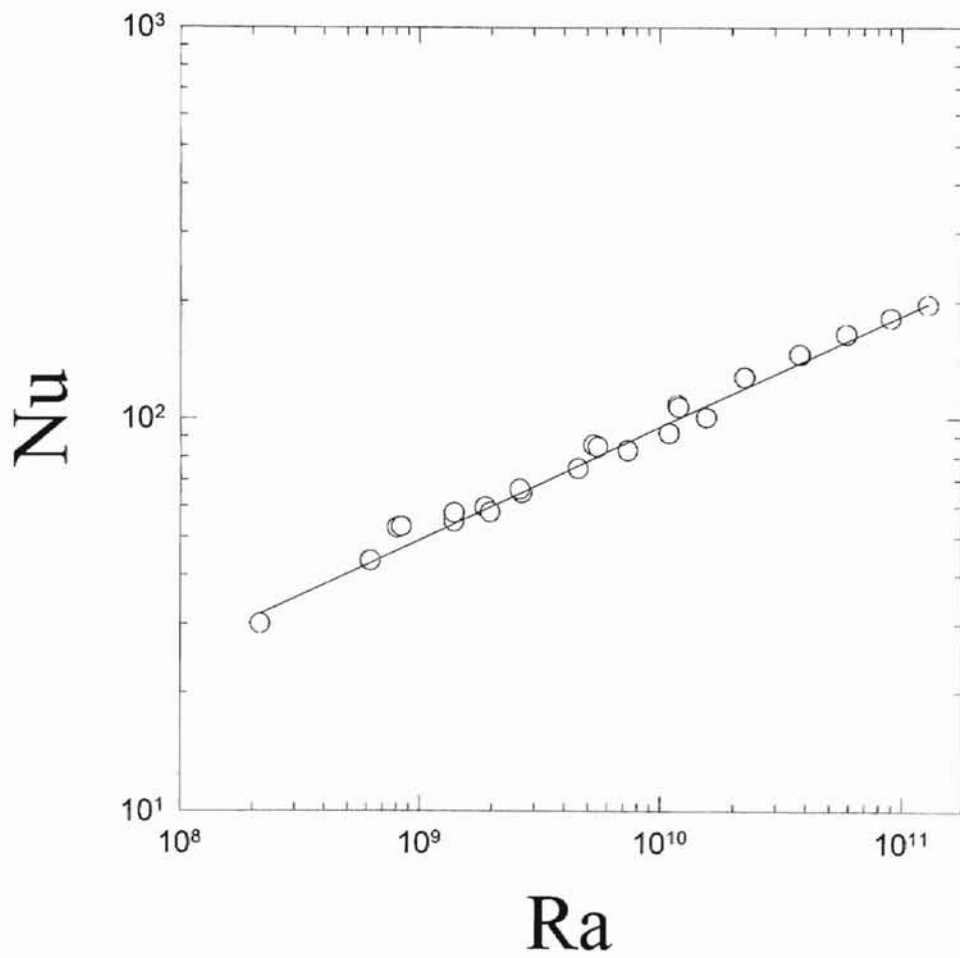


Figure 8. Measured  $Nu$  as a function of  $Ra$  in the smooth cells with  $A = 0.5$  and  $A = 1.0$ . The solid line is a power-law fit of  $Nu = 0.132 \times Ra^{0.286}$  to the open circles.

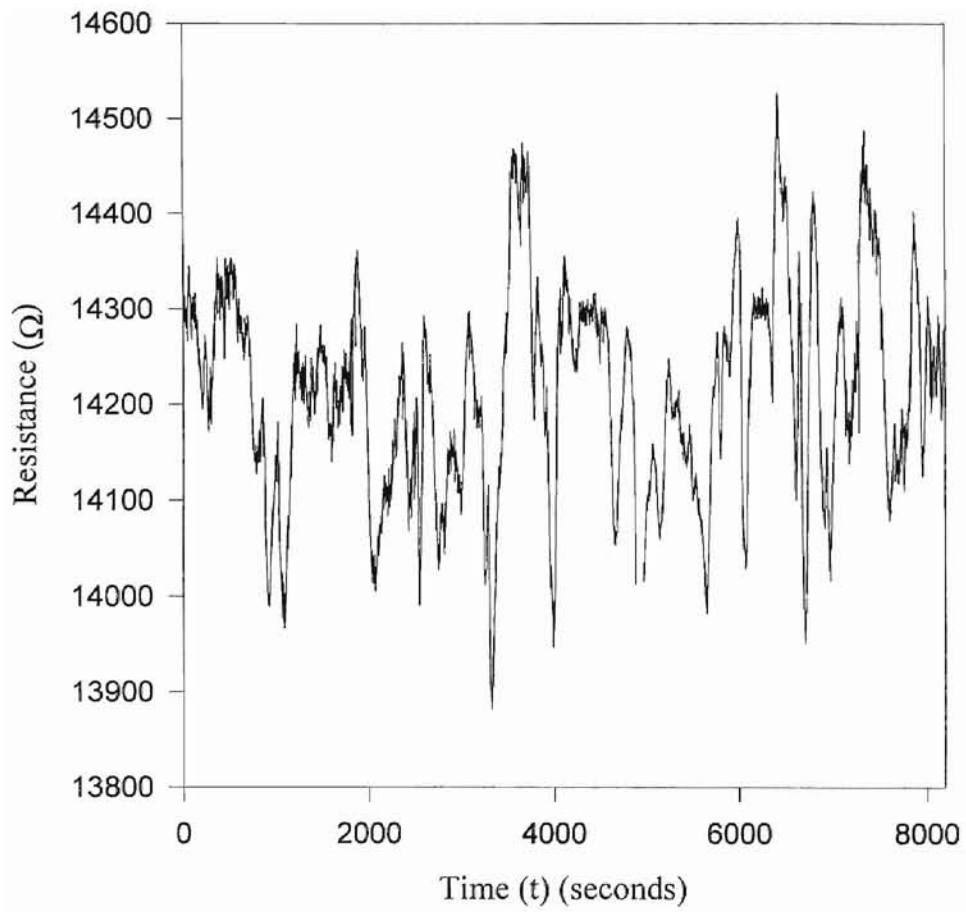


Figure 9. Resistance variations  $R_t$  with time  $t$  at the center of the cell when  $Ra = 1.39 \times 10^9$ .

previous measurements [5, 22]. Recent scaling theories for turbulent convection predict

$$\varepsilon = \frac{2}{7} [5,22].$$

Figure 9 shows variations of instantaneous fluid temperature  $T$  (in terms of resistance  $R$ ) with time  $t$  at  $Ra = 1.39 \times 10^9$ . As mentioned in the previous chapter, we originally acquired the data in the form of resistance, with the aid of the thermistor probe located at the center of the cell. The following equation was used to convert the resistance into temperature:

$$\frac{1}{T} = a + b \times \log R + c \times (\log R)^3 + d \times (\log R)^5 \quad (12)$$

where:  $a = 0.2527 \times 10^{-2}$

$$b = -0.2306 \times 10^{-3}$$

$$c = 0.3940 \times 10^{-4}$$

$$d = -0.7636 \times 10^{-6}$$

$R$  is the resistance in  $k\Omega$

$T$  is the temperature in  $^{\circ}\text{C}$ .

It is seen from Fig. 9 that the local temperature fluctuates strongly around its mean value in turbulent convection. To further study the statistics of temperature fluctuations, we compute the probability density function (PDF) of the measured temperature fluctuations. The PDF measures amplitude fluctuations of the measured temperature series ( $T$  vs.  $t$ ). Once again, we used LabVIEW to produce the PDF utilizing its extensive analysis libraries. The obtained PDF was then exported to a spreadsheet program.



Figure 10 shows a typical temperature PDF measured in the “smooth” cell with  $A=1.0$  when  $Ra = 1.09 \times 10^{10}$ . The measured PDF has an exponential shape and is essentially symmetric about the mean. It is interesting to note that the exponential decay lasts for approximately five decades, which requires a high statistical accuracy in the temperature measurements. This high statistical accuracy is another testament to LabVIEW’s versatility as a data acquisition and processing program.

Figure 11 illustrates how the temperature PDF changes with the Rayleigh number  $Ra$  when  $Ra$  is in the range between  $2.16 \times 10^8$  and  $1.09 \times 10^{10}$  in the  $A = 1$  cell. Note that the full width at half-maximum (FWHM), which is a measure of temperature variance, becomes narrower at higher Rayleigh numbers. This is expected because the turbulent mixing effect is enhanced. At high Rayleigh numbers (hard turbulence regime), local temperature fluctuations are homogeneous and isotropic, and their PDF in the central region has an invariant exponential form, with the rms temperature scaling with  $Ra$ . For the plots shown in Figures 10 and 11, the x-coordinate represents the temperature fluctuation  $\delta T = T - \bar{T}$ , normalized by the temperature difference  $\Delta T$  between the top and bottom plates. The y-coordinate is the logarithm of the probability. In such semi-log plots, an exponential function is represented by a simple straight line. The exponential PDF is found in both the “smooth” and “rough” cells with  $A = 1$ . For  $A \neq 1$  cells the measured PDF’s are no longer exponential. One possible reason is that the global circulation is not as stable as that in the  $A = 1$  cell. In the  $A = 0.5$  cell, we find that the measured PDF’s have a stretched exponential function form  $P \sim \exp [ -((T - \bar{T})/\Delta T)^{1.5} ]$ .

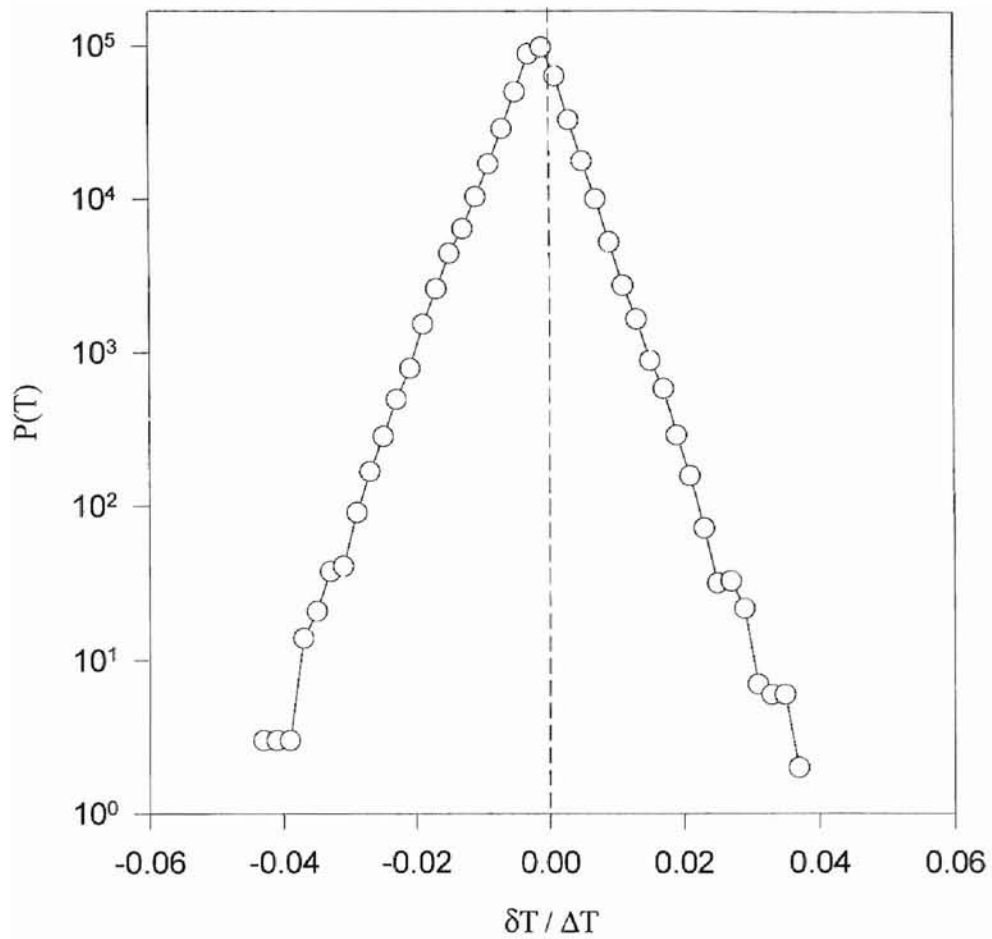


Figure 10. Measured temperature probability density function in the 20cm “smooth” cell at  $Ra = 1.09 \times 10^{10}$ .

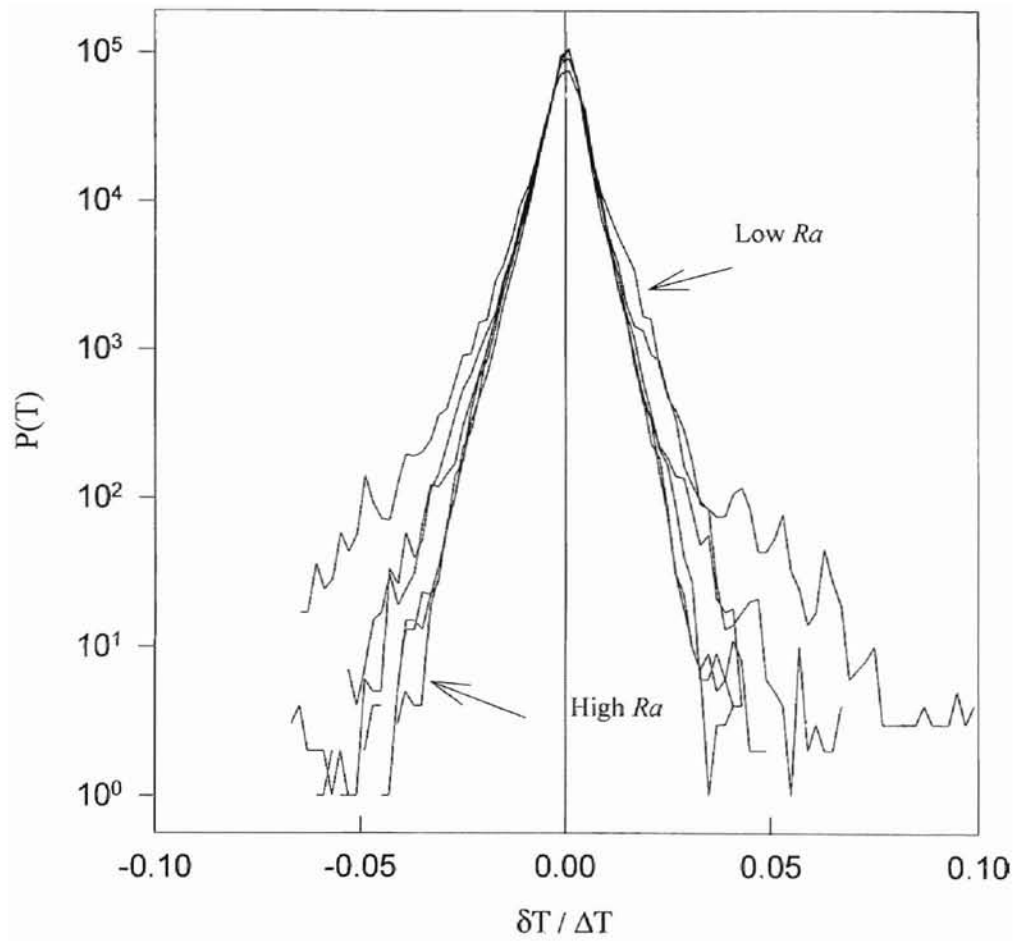


Figure 11. Measured temperature probability density function for different  $Ra$  ranging from  $2.16 \times 10^8$  to  $1.09 \times 10^{10}$ .

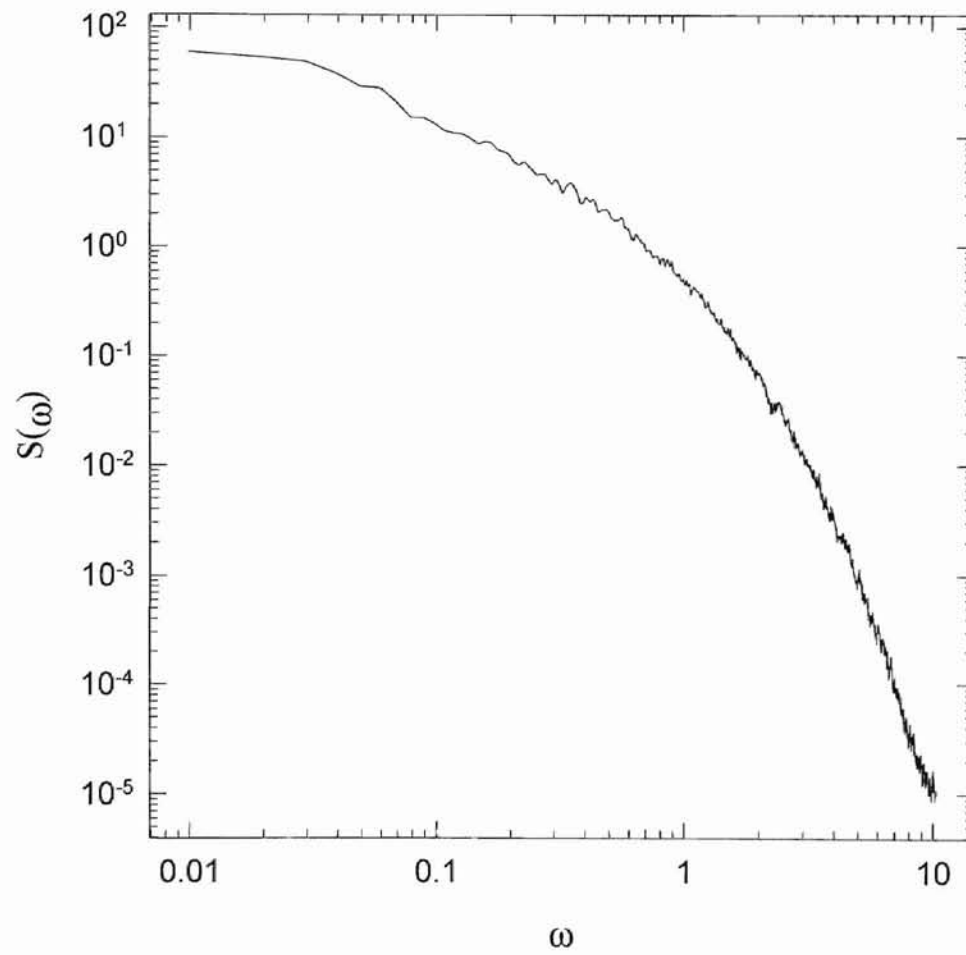


Figure 12. Measured power spectrum  $S(\omega)$  in the 20cm “smooth” cell at  $Ra = 1.09 \times 10^{10}$ .

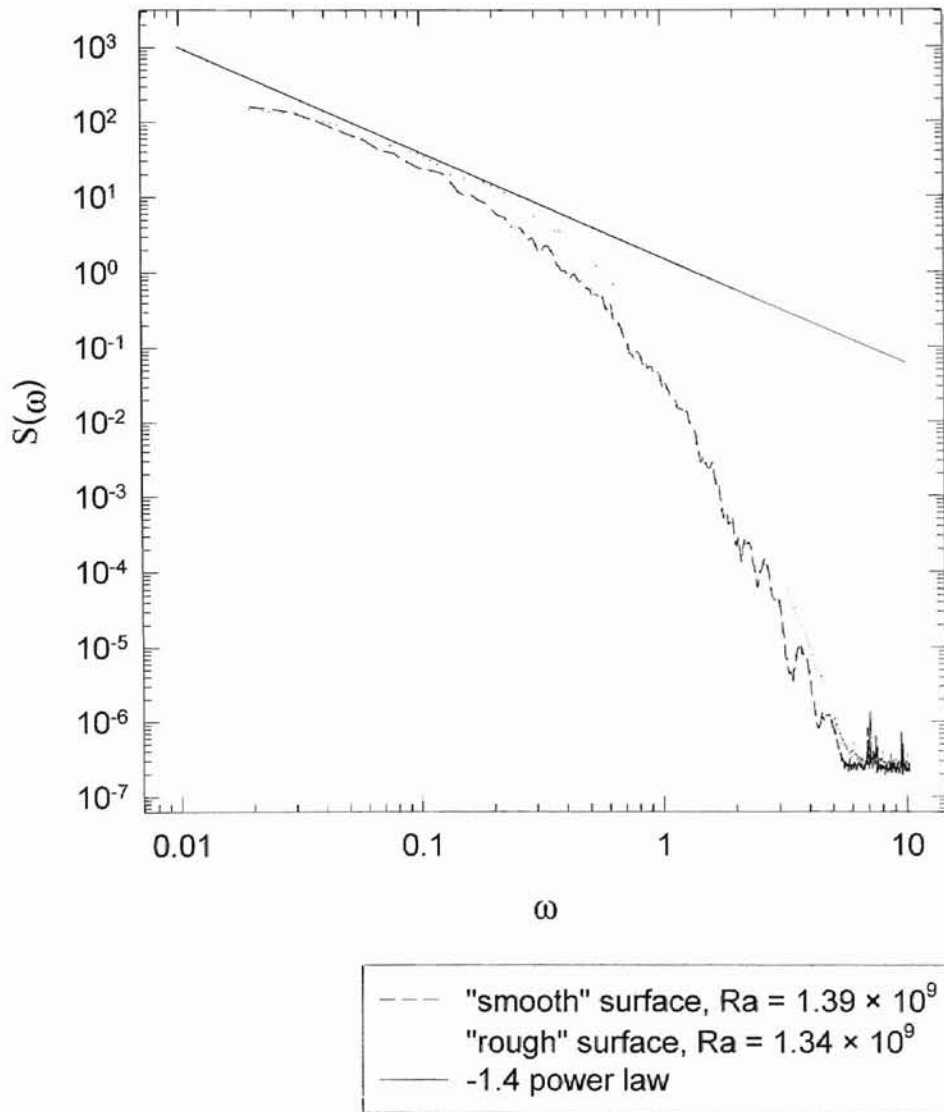


Figure 13. Measured power spectra  $S(\omega)$  for two different cells at approximately equal Rayleigh numbers.

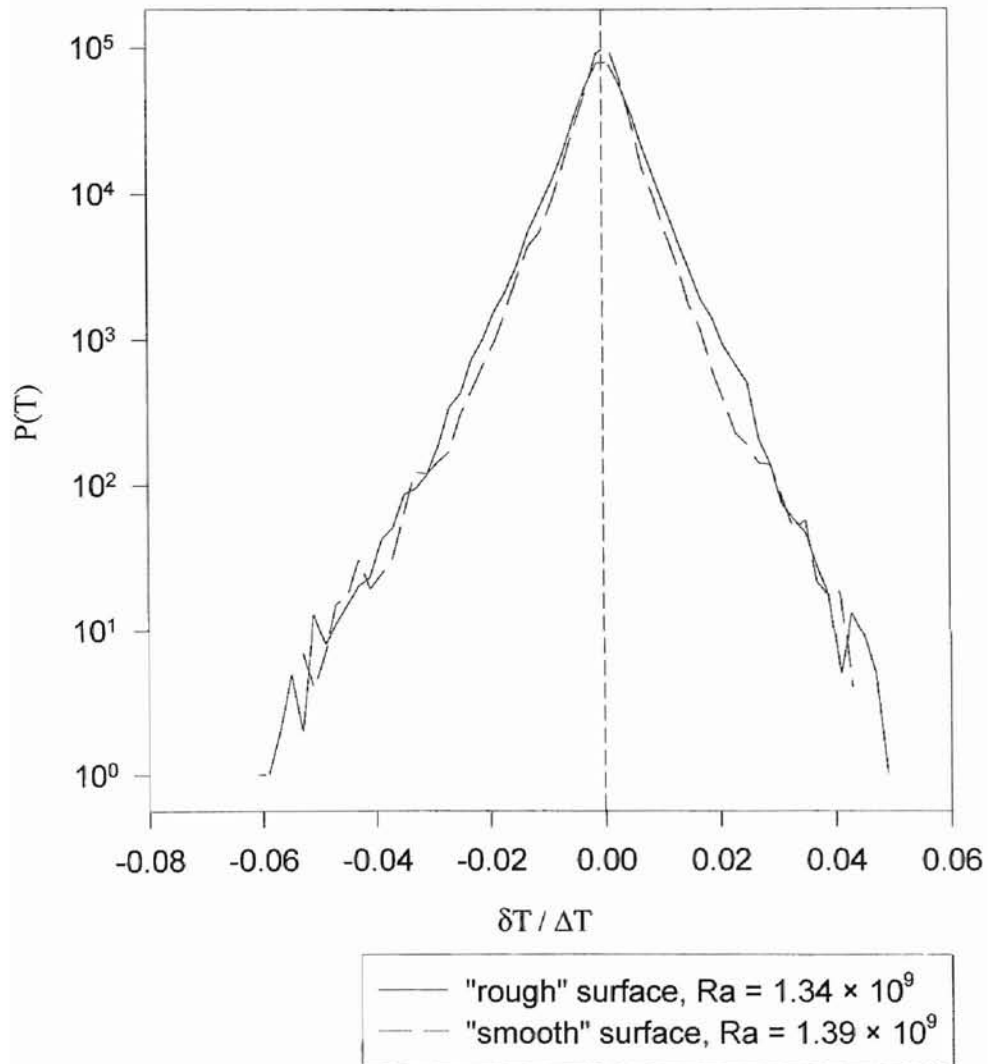


Figure 14. Measured temperature probability density functions in two different cells at approximately equal Rayleigh numbers.

To characterize the frequency response of temperature fluctuations in turbulent convection, we compute the power spectrum of the measured time series of temperature variations. Figure 12 shows a typical power spectrum measured in the “smooth” cell at  $Ra = 1.09 \times 10^{10}$ . The power spectrum is a Fourier transform of the temperature correlation function,  $\langle T(t)T(t+\tau) \rangle$ . Mathematically, the Fourier transform maps the time domain temperature variations  $T(t)$  into their frequency domain representation  $T(\omega)$  via

$$T(\omega) = \int_{-\infty}^{\infty} T(t) \exp(-i\omega t) dt. \quad (13)$$

The power spectrum  $S(\omega)$  is proportional to the squared modulus of the continuous Fourier transform  $T(\omega)$ , i.e.  $S(\omega) \sim |T(\omega)|^2$ . In the experiment, we used the data analysis package in LabVIEW to directly compute  $S(\omega)$  from the measured  $T(t)$ .

Figure 13 compares the power spectrum measured in the “smooth” cell ( $A = 1$ ) with that in the corresponding “rough” cell at approximately equal  $Ra$ . The Rayleigh number was  $Ra = 1.39 \times 10^9$  for the “smooth” cell (dashed line) and  $Ra = 1.34 \times 10^9$  for the “rough” cell (dotted line). Both of the power spectra exhibit similar low-frequency behavior. The flatness of the power spectra at low frequencies may be interpreted as a manifestation of a cutoff at the size of the cell. Moreover, the straight-line region of the power spectrum shows that there is a power law region developed between the flat low frequency cutoff and the sharp drop at high frequencies. The exponent of the power law is approximately  $-1.4$ , which is in good agreement with the results obtained by

Wu et al. [22]. For higher Rayleigh numbers, the range of this power law is increased. The “tail” part of the power spectra shown in Figure 13 has the stretched exponential form:

$$S(\omega) = S_h \exp(-(\omega/\omega_h)^\beta) \quad (14)$$

where  $S_h$ ,  $\omega_h$ , and  $\beta$  are parameters. Our data give  $\beta \approx 0.65$ . The stretched exponential decay of  $S(\omega)$  at high frequencies is a result of turbulent dissipation [22]. It is quite apparent that the functional form of the measured  $S(\omega)$  in the “rough” and “smooth” cells are very similar. This suggests that the “roughness” does not affect the cut-off frequency  $\omega_h$  in Eq.(14) very much. The “roughness” seems to have a more prominent effect on large-scale structures in the flow field and a lesser effect on the local mixing, especially at the center of the cell. But if we examine the graphs more carefully, we find that when  $A < 1$ , the “rough” cell data are always above the “smooth” cell data, indicating that turbulence is enhanced at all frequencies in the rough cells.

Figure 14 shows a comparison between the temperature PDF measured in the “smooth” cell and that in the “rough” cell at an approximately equal Rayleigh number. The full width at half-maximum (FWHM) in the “rough” cell is found to be somewhat wider than that in the “smooth” cell. Figure 14 thus indicates that the amplitude of temperature fluctuations is increased in the “rough” cell. The presence of the “rough”



surfaces in the convection cell produces larger temperature fluctuations, which result in a wider FWHM in the measured temperature PDF.

We also calculated the root mean square rms value of the temperature fluctuation  $\delta T(t)$  using LabVIEW. The temperature rms is defined as  $[\langle (T - \bar{T})^2 \rangle^{1/2}] / \Delta T$ , where  $\Delta T$  is the temperature difference between the top and bottom plates. It represents the width of the temperature PDF. Figure 15 shows the measured temperature rms as a function of the Rayleigh number in the rough cells. It is seen that the temperature rms in the  $A = 1$  cell is smaller than that in the  $A = 0.5$  cell. Because the global motion in the  $A = 0.5$  cell is not as stable as that in the  $A = 1$  cell, larger fluctuations in temperature are found in the  $A = 0.5$  cell. While the amplitude of temperature fluctuations in the rough cells is increased, the  $Ra$  of the measured temperature rms remains unchanged. The solid lines in Fig. 15 show the power fits to the data. The fitted with the exponent  $\beta = 0.12$  which is very close to that obtained in the smooth cell [23].

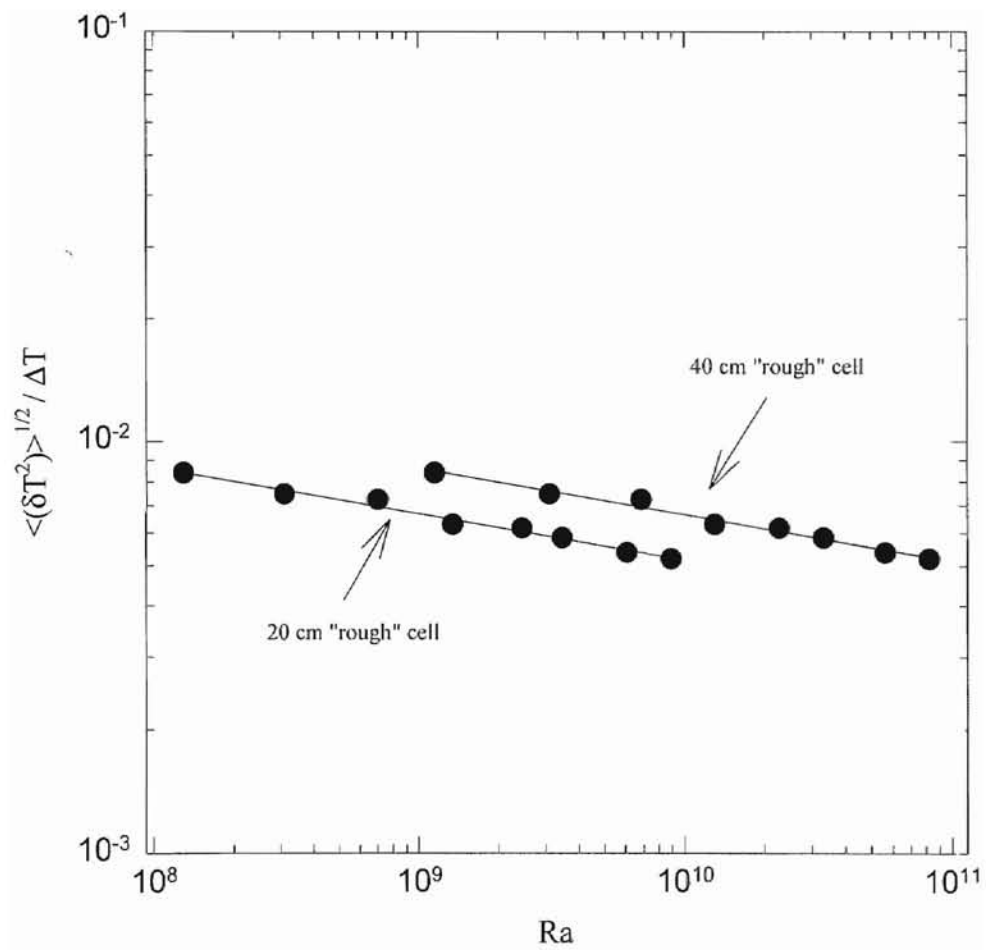


Figure 15. Measured temperature rms as a function of  $Ra$ .

# CHAPTER 4

## CONCLUSIONS

The purpose of this thesis was to study convective turbulence in an experimental system, in which one can precisely control the boundary conditions and change the flow state to a turbulent one in a systematic manner. The best candidate for such a system was Rayleigh-Bénard convection. There are three control parameters in Rayleigh-Bénard convection. They are the Rayleigh number  $Ra$ , the Prandtl number  $Pr$ , and the aspect ratio  $A = D / L$ , where  $D$  and  $L$  are the diameter and the height of the convection cell, respectively.

The experimental aspect of this study proved to be quite challenging. After setting up the experimental apparatus, which consisted, among other things, of convection cells of different aspect ratios as well as inner top and bottom surfaces (including both “smooth” and “rough” ones), a significant amount of time and effort was devoted on designing a sophisticated yet user-friendly data acquisition system. This was accomplished with the aid of AT-GPIB/TNT™ interface boards and LabVIEW®, a powerful graphical language package with extensive statistical libraries. The preparation of all the elements pertinent to data acquisition greatly facilitated the successful completion of this project. Several *virtual instruments* were designed to interface with the actual physical instruments, thereby enabling almost instantaneous data acquisition and processing on a personal computer.

The collected data of temperature fluctuations  $\delta T(t)$  in turbulent convection were thoroughly analyzed by means of the temperature probability density function (PDF)  $P(\delta T)$ , the root mean square value,  $\langle(\delta T)^2\rangle^{1/2}$  and the power spectrum  $S(\omega)$ . It is found that in the “smooth” cell, the temperature PDF has an invariant exponential form which is in good agreement with results obtained by Heslot et al [5]. In the central region of the “rough” cell, temperature fluctuations are found to be enhanced, but their PDF has the same functional form as the one for the “smooth” cell. The rms values are increased considerably in the  $A = 0.5$  cell, in which the large-scale circulation is found to be unstable. The power spectrum  $S(\omega)$  measured in the “rough” cell is found to have a stretched exponential tail, given by the expression  $S(\omega) \sim \exp(-(\omega/\omega_h)^{0.65})$ . A similar power spectrum is also found in the “smooth” cell.

## BIBLIOGRAPHY

1. M. Bénard, *Ann. de Chimie et de Physique*, **23**, 62 (1901).
2. E. S. C. Ching, *Phys. Rev. A* **44**, 3622 (1991).
3. E. S. C. Ching, *Phys. Rev. Lett.* **70**, 283 (1993).
4. T. E. Faber, *Fluid Dynamics for Physicists*, (Cambridge University Press, Cambridge 1995).
5. F. Heslot, B. Castaing, and A. Libchaber, *Phys. Rev. A* **36**, 5870 (1987).
6. I. Hosokawa, *Phys. Rev. E* **49**, R4775 (1994).
7. Keithley Application Note 2001, Model 2001: High-Performance Digital Multimeter, June 1993.
8. Keithley Application Note 199, Model 199 Quick Reference SCPI Guide, March 1991.
9. A. N. Kolmogorov, *C. R. Dokl. Acad. Sci. USSR* **30**, 301 (1941); **31**, 538 (1941).
10. A. Khurana, *Physics Today*, **17**, June 1988.
11. National Instruments Application Note 040, *Fast Fourier Transforms and Power Spectra in LabVIEW<sup>®</sup>*, National Instruments Corporation Press, February 1993.
12. National Instruments' *LabVIEW<sup>®</sup> for Windows User Manual*, National Instruments Corporation Press, December 1993.
13. National Instruments' *LabVIEW<sup>®</sup> for Windows Analysis VI Reference Manual*, National Instruments Corporation Press, December 1993.

14. National Instruments' *Getting Started with Your AT-GPIB/TNT and the NI-488.2™ Software for DOS*, National Instruments Corporation Press, December 1993.
15. L. Rayleigh, *Phil. Mag.* **32**, 529 (1916)
16. M. R. Raupach, R. A. Antonia, and S. Rajagopalan, *Appl. Mech. Rev.* **44**, 1 (1991).
17. Y. Shen, Ph. D. Thesis, Oklahoma State University, January 1996.
18. T. H. Solomon, and J. P. Gollub, *Phys. Rev. Lett.*, **64**, 2382 (1990).
19. A. Tilgner, A. Belmonte, and A. Libchaber, *Phys. Rev. A* **45**, 842 (1992).
20. P. Tong, and Y. Shen, *Phys. Rev. Lett.* **69**, 2066 (1992).
21. D. J. Tritton, *Physical Fluid Dynamics*, second edition (Clarendon press, Oxford, 1988).
22. X.-Z. Wu, L. Kadanoff, A. Libchaber, and M. Sano, *Phys. Rev. Lett.* **64**, 2140 (1990).
23. X.-Z. Wu, and A. Libchaber, *Phys. Rev. A* **64**, 842 (1992).
23. X.-Z. Wu, Ph. D. Thesis, The University of Chicago, June 1991.
24. G. Zocchi, E. Moses, and A. Libchaber, *Physica A* **166**, 387 (1990).

VITA

George Kambouroglou

Candidate for the Degree of

Master of Science

Thesis: A STUDY OF TEMPERATURE FLUCTUATIONS AND THEIR STATISTICS  
IN TURBULENT CONVECTION

Major Field: Physics

Biographical:

Personal Data: Born in Thessaloniki, Greece, on July 29, 1971, the son of Jordan and Lina Kambouroglou.

Education: Graduated from Anatolia College High School, Thessaloniki, Greece in May 1993; received Bachelor of Arts degree in Physics from Illinois Wesleyan University, Bloomington, Illinois, May 1993; completed requirements for the Master of Science degree at Oklahoma State University, August 1997.

Professional Experience: Teaching Assistant, Department of Physics, Oklahoma State University, August 1993 to December 1996; Research Assistant, Department of Physics, Oklahoma State University, June 1994 to December 1994.

Professional Memberships: American Physical Society, Society of Physics Students.